scientific reports

Check for updates

OPEN

MIEN1 promoter deletion leads to impaired migration and invasion potential via actin cytoskeleton rearrangement in colorectal cancer

Payal Ranade[1], Rucha Trivedi[1], Diana Carolina Sierra-Díaz[2], Paul Laissue[3] & Jamboor K. Vishwanatha[1]✉

Colorectal cancer (CRC) is a leading cause of cancer-associated mortality worldwide. Although early-stage CRC is responsive to surgical resection, advanced metastatic disease poses formidable treatment obstacles, triggering an alarming decline in the survival rates of patients. Hence, studying the mechanisms underlying CRC progression and identifying novel therapeutic targets are critical for early diagnosis and treatment. The migration and invasion enhancer 1 (MIEN1) protein plays a pivotal role in tumor invasion and migration across various cancer types. In CRC, the predominant upregulation of MIEN1 in cancerous tissues is closely associated with invasive behavior; however, the precise mechanism driving the metastasis remains unexplored. In this study, we investigate the role of MIEN1 in CRC by generating a CRISPR-Cas9 mediated promoter knockout in HT29 CRC cell-line. The effects of *MIEN*1 deletion on critical biological processes and molecular pathways, including cell adhesion, migration, and invasion, were investigated using functional assays. RNA sequencing analysis indicated alterations in actin cytoskeleton rearrangement, ultimately manifesting as differences in cellular migration and invasion potential. Signaling molecules essential for actin remodeling, such as phosphorylated FAK (pFAK-Y397) and phosphorylated cofilin (pCofilin-S3), exhibited distinct differences in their cellular localization, implicating the role of MIEN1 in modulating these key proteins. Our findings emphasize the involvement of MIEN1in diverse signaling pathways responsible for CRC migration, with its deletion leading to the disruption of several biological processes, particularly actin cytoskeleton rearrangement, which is crucial for metastasis. Therefore, targeting MIEN1 may be an effective therapeutic strategy against CRC.

Colorectal cancer (CRC) is the third most common cancer diagnosed globally and is one of the leading causes of cancer-associated mortality. Its progression is classified into four stages, with stages 3 and 4 being marked by an increased rate of malignancy[1,2]. If the cancer is diagnosed in the early stages, the tumor can be removed surgically; however, as the tumor gains metastatic ability, the overall survival rate of patients decreases drastically. Therefore, understanding the molecular mechanisms underlying CRC progression, which ultimately leads to metastasis, is crucial for developing effective therapeutic strategies.

Metastasis begins with the migration and invasion of cancer cells from the original tumor site to a distant organ. This process involves complex interactions between the signaling pathways and various proteins. Migration and invasion enhancer 1 (MIEN1) is an important protein involved in this process. Previously the protein was referred to by other names, such as C17orf37 and C35. The gene for this protein is located on chromosome 17q12 positioned between *ERBB2* oncogene and *GRB7* in a tail-to-tail orientation, adjacent to the ERBB2/HER2 oncogene. It encodes a 112-amino acid protein of 15kD. Unlike many oncogenes driven by gene amplification, *MIEN1* overexpression appears to be primarily regulated at the transcriptional level, including epigenetic changes such as promoter hypomethylation. The MIEN1 protein is overexpressed across various cancer types, significantly augmenting invasive and migratory phenotypes in breast, prostate, oral, and non–small cell lung cancers[3–5], but has no detectable expression in normal or noncancerous adjacent tissues.

[1]Department of Microbiology, Immunology and Genetics, University of North Texas Health Science Center, Fort Worth, TX, USA. [2]Center for Research in Genetics and Genomics (CIGGUR), Institute of Translational Medicine (IMT), School of Medicine and Health Sciences, Universidad del Rosario, Bogotá, Colombia. [3]Biopas Laboratoires, Rare Diseases Unit, BIOPAS GROUP, 111111 Bogotá, Colombia. ✉email: jamboor.vishwanatha@unthsc.edu

Immuno-histochemical analysis of CRC patient samples showed similar MIEN1 overexpression, which is associated with cancer aggressiveness and metastasis[6].

In this study, we elucidated the role of MIEN1 in CRC by employing promoter knockout studies to harness its potential for therapeutic intervention. Using the highly tumorigenic HT29-human colorectal carcinoma cell line, we generated a stable *MIEN1* knockout cell line using CRISPR-Cas9 gene editing technology. We characterized the resulting phenotypic alterations and gene expression changes to elucidate the role of MIEN1 in CRC cell migration and invasion. Additionally, we examined the effects of MIEN1 knockout on actin cytoskeleton dynamics, which are pivotal determinants of cell migration. Our findings demonstrate the critical involvement of MIEN1 in CRC cell migration and invasion.

Results

CRISPR-Cas9–mediated *MIEN1* promoter ablation does not affect *ERBB2* amplicon

MIEN1 is positioned between *GRB7* and *ERBB2* in a tail-to-tail orientation, adjacent to the *ERBB2/HER2* oncogene (Fig. 1A). Its expression is regulated transcriptionally rather than through alterations in the copy number of the associated amplicon[7,8]. Hence, to investigate the effect of the MIEN1 protein on CRC cell migration and invasion, we used the CRISPR-Cas9 technology to knock out its promoter region, ensuring that the *ERBB2* amplicon remained unaffected.

Deletion of the minimal promoter region of 856 base pairs (bp) upstream of the ATG start codon (+1 position) (Fig. S1) for *MIEN1* in HT29 human CRC cells was confirmed by sequencing genomic DNA from a single-cell clone (Fig. 1B) after puromycin selection. The cell line lacking the *MIEN1* promoter region was named HT29-pMIEN1-X (referred to as HT29 KO).

Reverse transcriptase polymerase chain reaction (RT-PCR) in both HT29 cell variants, showed minimal *MIEN1* transcript levels in the HT29 KO cells. Additionally, a minor PCR product of approximately 300 bp, corresponding to *GAPDH*, resulted in an ambiguous PCR product, likely because of nonspecific primer binding. (Fig. 1C). To further validate the knockout at the protein level, immunoblotting was performed, which confirmed the complete absence of the MIEN1 protein in knockout cells, whereas wild-type (WT) cells had abundant levels of the protein (Fig. 1D).

To verify whether *MIEN1* promoter deletion affected neighboring genes, we performed immunoblot analysis of ErbB2 and GRB7 proteins and observed no changes in their expression (Fig. 1D). Additionally, to confirm the establishment of a stable HT29 KO cell line, we performed immunoblot analysis of MIEN1 and the proteins encoded by the neighboring genes across multiple passages. Our observations indicated a consistent absence of MIEN1 protein in HT29 KO cells, with unaltered expression in HT29 WT cells throughout numerous subcultures

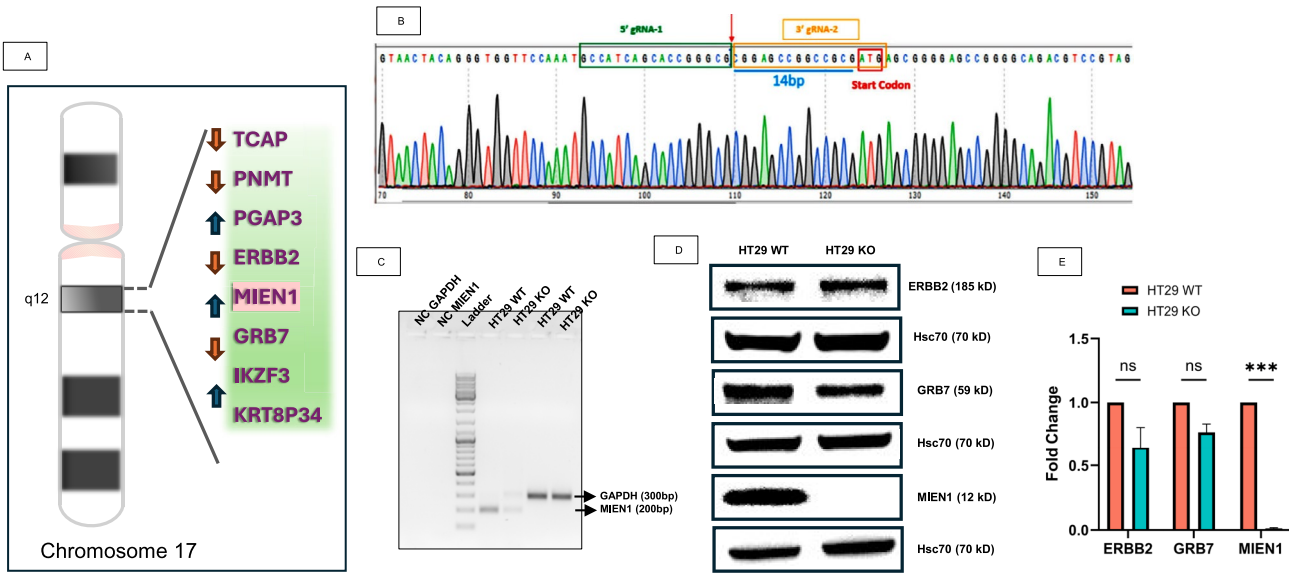

Fig. 1. *MIEN1* promoter knockout and cell line characterization. (**A**) Schematic representation of chromosome 17 of the human genome, depicting the location of the *MIEN1* gene. (**B**) Genomic DNA sequencing of HT29 cells following the deletion of the *MIEN1* promoter region. (**C**) Reverse transcriptase polymerase chain reaction of *MIEN1* in both HT29 cell variants, WT and KO, observed at 200 bp, and the *GAPDH* gene observed at 300 bp as a control. (**D**) Western blot image representative of the whole-cell lysate of HT29 WT and KO cells showing the expression of MIEN1, ErbB2, and GRB7 proteins, which represent the protein products of genes adjacent to *MIEN1*. The Hsc70 protein was used as a loading control. (**E**) Quantification of the band density of western blot images for proteins to compare HT29 WT and KO cell expression. The paired t-test was used to perform statistical analysis, with n = 5 in each group. ns, non-significant; ***, $p < 0.0005$; MIEN1, migration and invasion enhancer 1; bp, base pairs; WT, wild-type; KO, knockout.

(Fig. 1E). Moreover, no substantial reduction in the expression of proteins encoded by the neighboring genes *ERBB2* and *GRB7* was observed over successive passages (Fig. 1E).

Collectively, these results confirmed the establishment of a stable *MIEN1* knockout in HT29 cells and indicated a lack of impact on neighboring genes, such as *ERBB2* and *GRB7*.

MIEN1 knockout results in transcriptomic alterations

To understand the alterations in gene expression patterns following the knockout of *MIEN1*, mRNA sequencing was performed. Principal component analysis (PCA) revealed distinct expression profiles, with PC1 accounting for 56% of the variance, highlighting significant global differences in gene expression (Fig. 2A). Differential expression analysis revealed that, out of 1262 differentially expressed genes in HT29 KO cells, 494 genes were upregulated with a fold change greater than 1.0, whereas 768 genes were downregulated with a fold change of less than 1.0, with a *P*-value cut-off of 0.05 (Fig. 2B).

Using ingenuity pathway analysis (IPA; Qiagen), we identified the key pathways and biological processes affected by *MIEN1* knockout. Among the disease pathways predicted by machine learning, tumor growth has been highlighted as one of the major inhibited pathways. Several key processes, such as the extension of cellular protrusions, movement of tumor cells, ruffling, transactivation, immortalization, and invasion of tumor cells, were predicted to be suppressed (Fig. 2C). Three major pathways—CRC metastasis signaling, regulation of epithelial-mesenchymal transition (EMT) by the growth factor pathway, and the tumor-microenvironment (TME) pathway—were among the downregulated canonical pathways. The CRC metastasis signaling pathway revealed that cell proliferation and survival are inhibited by the Wnt signaling pathway. Apoptosis was highlighted as an activated process, whereas migration, metastasis, cell proliferation, and angiogenesis were predicted to be indirectly inhibited because of stunted growth factor signaling in colorectal tumorigenesis (Fig. S2). In the regulation of EMT by the growth factor pathway, cytoskeleton reorganization, which indirectly influences migration, cell invasion, and disassembly of cell–cell junctions, was suppressed through receptor tyrosine kinase signaling. This suppression resulted in the overall inhibition of the EMT process, significantly affecting cell migration, lesion healing, and metastasis. Similarly, transforming growth factor-β (TGF-β) signaling was predicted to inhibit the overall EMT process, further suppressing cell invasion, migration, lesion healing, and metastasis. Cell–cell adhesion was predicted to be activated via both receptor tyrosine kinase and TGF-β signaling (Fig. S3). The TME pathway has also been predicted to inhibit tumor cell invasion and metastasis. In contrast, tumor cell proliferation, survival, angiogenesis, and apoptosis were predicted to be activated (Fig. S4).

IPA also highlighted a range of biological processes affected by *MIEN*1 knockout, including disruptions in cell signaling, cellular movement, molecular transport, tumor morphology, and cellular assembly and organization (Fig. 2D). The clustered bar graph in Fig. 2E highlights the molecular and cellular processes affected by *MIEN1* knockout. Cell movement and migration, tumor frequency, transdifferentiation, cell invasion, tumor incidence, EMT, tumor cell proliferation, actin filament quantity, and cytoskeletal rearrangement had negative Z-scores, indicating inhibition, whereas tumor cell death, necrosis, apoptosis, and cell–cell adhesion were predicted to be activated, with positive Z-scores.

Overall, IPA analysis emphasized that the knockout of *MIEN1* in HT29 cell line significantly impaired critical processes, such as migration, invasion, and cytoskeleton rearrangement, while promoting cell–cell adhesion and apoptosis.

MIEN1 deletion alters actin cytoskeleton rearrangement

Gene ontology enrichment analysis indicated that *MIEN1* knockout negatively affected cell motility, migration, locomotion, and the formation of membrane ruffles (Fig. S3). Cell migration is a complex process orchestrated by the coordinated polymerization of actin filaments, leading to the formation of protrusive structures, known as lamellipodia, at the leading edges of migratory cells. Previously, we demonstrated the pivotal role of the actin cytoskeleton in prostate and breast cancer metastases.[3,4] HT29 WT cells displayed enhanced staining at their cell peripheries, suggesting the formation of lamellipodium ruffles, along with fewer stress fibers within the cell body, indicating decreased cell adhesion (Figs. 3A, S5, S6 and S13). Conversely, HT29 KO cells exhibited a notable accumulation of stress fibers across their cell bodies and minimal F-actin build-up at the cell periphery, signifying enhanced cellular adhesion and reduced motility (Figs. 3C, S7, S8 and S14). The distance-versus-phalloidin intensity graphs corroborated our findings, revealing a three-fold increase in phalloidin intensity at the cell peripheries of WT cells compared to that in their cell bodies (Figs. 3B, S9, S10 and S15). This suggests the presence of lamellipodia at the cell edges and fewer stress fibers in the cell body. Conversely, the knockout cells displayed increased intensities uniformly across the entire cell, indicating the prevalence of stress fibers throughout the cell and the absence of lamellipodium ruffles (Figs. 3D, S11, S12 and S16).

When examining the phalloidin staining pattern along the cell edges, we observed that phalloidin intensity increased exponentially, maintaining a steady level within a specific distance range. This indicated increased intensity, specifically in the lamellipodium region, tapering off on either side of the WT cells (Figs. 3E and S17). In contrast, the edges of the knockout cells displayed a graph similar to that observed in the cell body, showing irregular staining patterns and distinctly emphasizing the absence of lamellipodium ruffles (Figs. 3F and S18).

Phosphorylation of essential actin cytoskeleton proteins FAK and cofilin is altered owing to the absence of MIEN1

To validate actin cytoskeleton impairment in HT29 KO cells, we examined the key actin cytoskeleton proteins—FAK and cofilin, specifically their phosphorylated forms, pFAK-Y397 and pCofilin-S3 by immunofluorescent staining and immunoblotting. In WT cells, pFAK-Y397 was localized to the cellular edges where lamellipodium ruffles were evident, whereas in HT29 KO cells, pFAK was present within the stress fibers in the cell body (Fig. 4A). Upon quantifying the fluorescence intensity of pFAK-Y397 , we observed a 2.5-fold higher localization

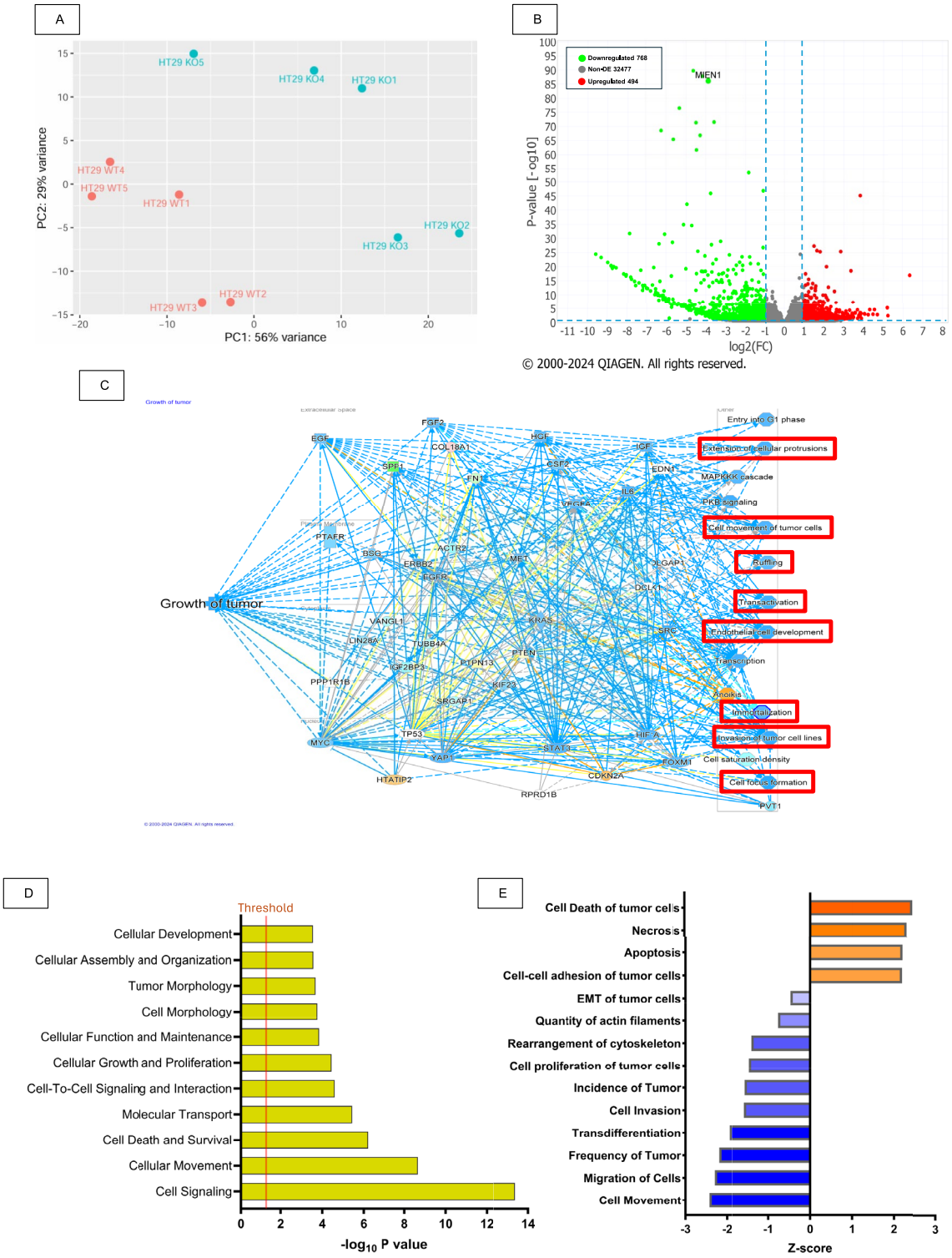

of pFAK-Y397 at the cell periphery in WT cells compared to *MIEN1* KO cells. Whereas *MIEN1* KO cells exhibited a pronounced 20-fold increase in pFAK-Y397 localization within the cell body compared with that of WT cells (Fig. 4B). These quantifications clearly illustrate the disruption in the distribution pattern of active FAK upon *MIEN1* knockout. WT cells, with significantly higher peripheral pFAK, reflect active focal adhesions at the cell edge, a hallmark of efficient migration. Conversely, the substantial increase of active FAK in the cell body in *MIEN1* KO cells indicates mislocalization, potentially causing impaired focal adhesion dynamics and inhibited cell motility. Immunoblotting analysis showed a significant reduction in the pFAK Y397 to total FAK ratio compared to WT cells, indicating decreased FAK activation. (Fig. 4E and F).

Cofilin, an actin-depolymerizing protein, is inactivated upon phosphorylation at the serine residue in the third position. Staining for pCofilin-S3 showed a higher intensity in HT29 KO cells than in WT cells (Fig. 4C). Quantification of fluorescence intensity showed a 40% increase in KO cells compared with that in

◀**Fig. 2**. HT29 mRNA sequencing and enrichment analysis. (**A**) Principal component analysis depicting expression patterns between HT29 WT and KO cells, with PC1 capturing the variance between the two groups and PC2 capturing the variance in each group. (**B**) Volcano plot, with each symbol depicting each gene identified in mRNA sequencing. The gray points represent genes with log2[fold change] in the range of − 1.0 to + 1.0. Data points in green represent genes downregulated upon *MIEN1* knockout with log2[fold change] less than- 1.0, and those in red represent genes upregulated upon *MIEN1* knockout with log2[fold change] greater than + 1.0. (**C**) Growth tumor pathway showing various processes with predicted inhibition (blue) or activation (orange). Processes of interest are outlined in red. (**D**) Bar graph representing the processes that were significantly modulated upon *MIEN1* knockout. The − log10[*P*-value] indicates the extent of significance, as observed using the entire mRNA sequencing dataset. (**E**) Clustered bar graph showing the subset of functional processes observed relevant to this study derived from IPA software. The PCA plot, volcano plot, and pathway analysis were generated using IPA software, and bar graphs were generated using GraphPad Prism 10 software. PCA, principal component analysis; IPA, ingenuity pathway analysis; MIEN1, migration and invasion enhancer 1; WT, wild-type; KO, knockout; TME, tumor microenvironment; EMT, epithelial-mesenchymal transition.

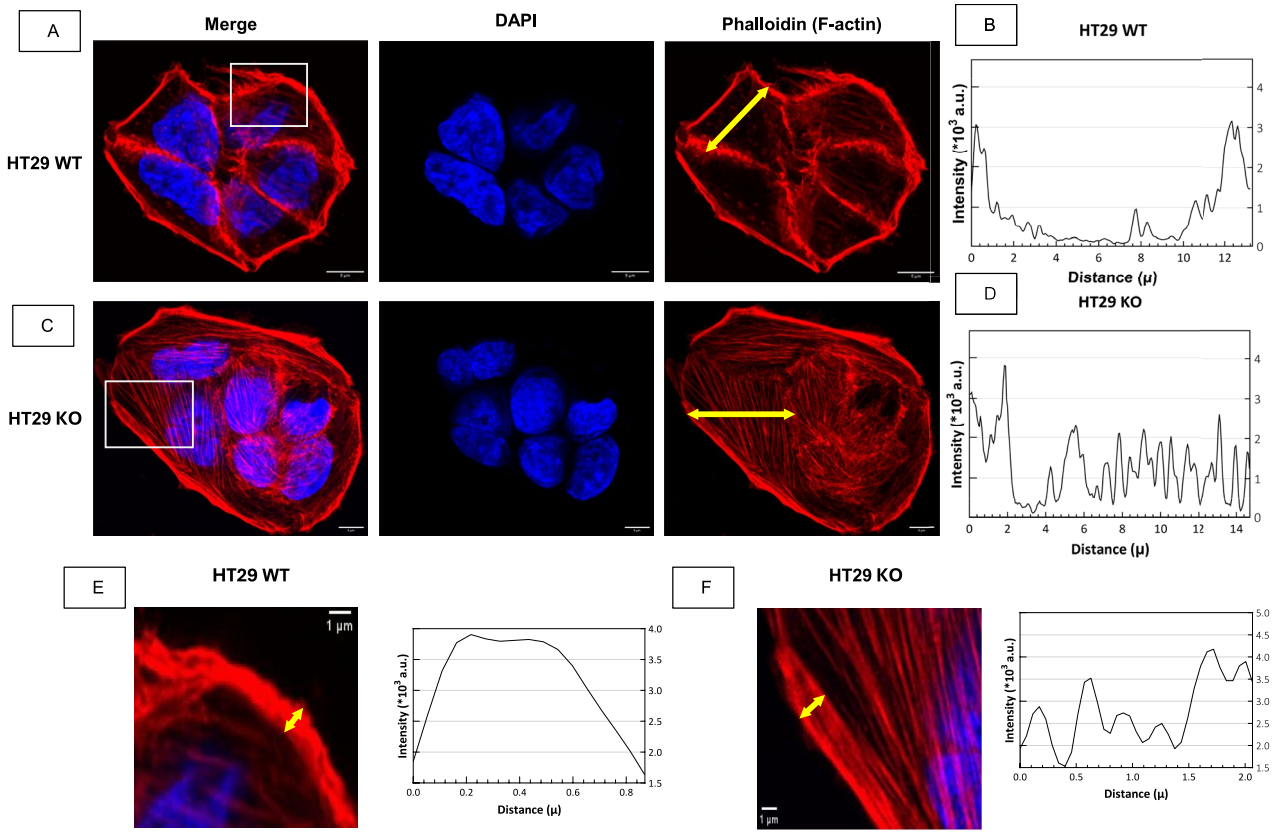

Fig. 3. Effect of *MIEN1* knockout on actin cytoskeleton structure. (**A** and **C**) Immunofluorescence microscopy images showing phalloidin staining of F-actin in HT29 WT and KO cells. The first column shows a merged image of the DAPI nuclear stain (second column) and phalloidin stain (third column). (**B** and **D**) Fluorescence intensity of the image around the yellow arrow (phalloidin, third column) is represented in the graph. (**E** and **F**) Images represent zoomed sections of the merged images from Fig. 3A and C (first column, gray box) with their respective intensities of the area indicated by the yellow arrow on the edge of the cells. Images were acquired using the Zeiss LSM 880 Confocal with Airyscan microscope at 63 × magnification. Fluorescence intensities were measured using ImageJ software. Scale bars: 5 μm (3A and C), 1 μm (3E and 3F). WT, wild-type; KO, knockout; MIEN1, migration and invasion enhancer 1.

WT cells (Fig. 4D). Immunoblotting for cofilin and its phosphorylated form at S3 showed a visible increase in phosphorylated Cofilin levels., although the pCofilin/Cofilin ratio showed an upward trend in KO cells relative to WT. While the pCofilin/Cofilin ratio exhibited an upward trend compared to WT, the difference did not reach statistical significance (Fig. 4E and F). These observations demonstrated cofilin inactivation upon MIEN1 knockout, suggesting decreased actin depolymearization.

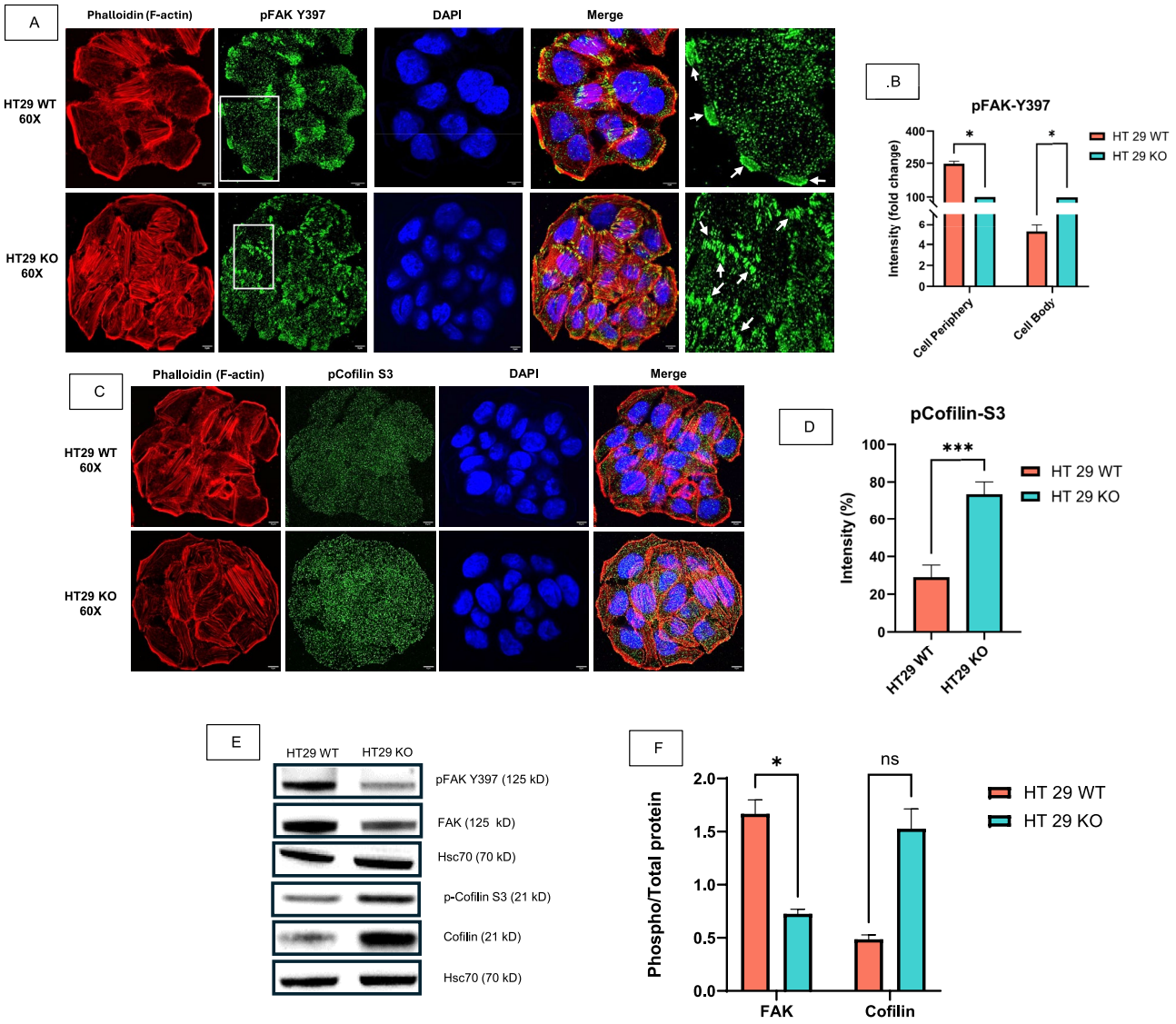

Fig. 4. *MIEN1* knockout modulates key actin cytoskeleton proteins. (**A**) Immunofluorescence staining images of the actin cytoskeleton and pFAK. (**B**) Quantification of the intensity of pFAK-Y397 at the cell periphery and in the cell body of the same images, performed using ImageJ software. The paired t-test was used to compare the groups, with n = 2 in each group. (**C**) Immunofluorescence staining images of the actin cytoskeleton and pCofilin-S3. (**D**) Quantification of the intensity of pCofilin-S3 in HT29-WT and KO cells, performed using ImageJ software. The two-tailed unpaired t-test was used to compare the groups, with n = 6 in each group. (**E**) Western blot image representative of the whole-cell lysate of HT29 WT and KO cell lines, showing the expression of key cytoskeletal proteins, with Hsc70 as a control. (**F**) Quantification of the band density of western blot images for proteins to compare HT29 WT and KO cell expression, as performed using the ImageJ software. The paired t-test was used to perform statistical analysis, with n = 3 in each group. GraphPad Prism 10 was used to generate the graph and perform statistical analysis, with *, $p < 0.05$; **, $p < 0.005$; ***, $p < 0.0005$. Images were acquired using the Zeiss LSM 880 Confocal with Airyscan microscope at 63 × magnification. Fluorescence intensities were measured using ImageJ software. MIEN1, migration and invasion enhancer 1; KO, knockout; WT, wild-type.

Collectively, our data provides evidence of impaired actin cytoskeleton dynamics, which are critical for cell motility machinery (lamellipodia and filopodia), in the absence of MIEN1 protein. These results emphasize the importance of MIEN1 in CRC cell migration.

MIEN1 knockout affects the migration and invasion potential of CRC cells

We performed various functional assays to validate the observed changes in the actin cytoskeleton. Cell–cell adhesion was evaluated using the hanging-drop experiment. HT29 KO cells formed single spheroids within 24 h of incubation. In contrast, HT29 WT cells required more than 72 h to form a single spheroid, along with multiple smaller cell aggregates. By day 4, HT29 KO cells formed elliptical spheroids with a distinct border and a denser

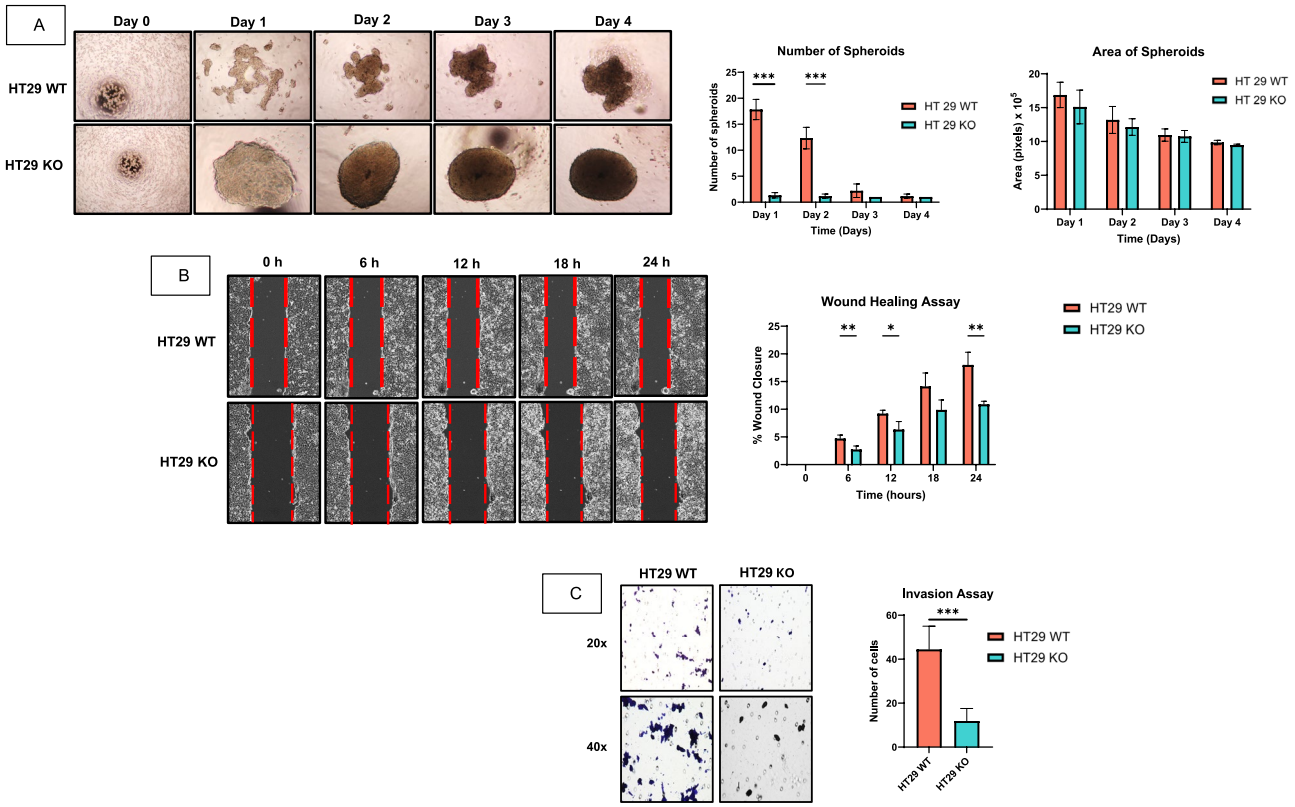

Fig. 5. Migratory and invasive potential of HT29 cells is reduced upon *MIEN1* knockout. (**A**) Representative brightfield microscopy images of spheroids from days 0 to 4 in HT29 WT and KO cells. The number of spheroids formed each day was quantified manually and is represented by a bar graph. A multiple comparison test was performed to analyze the statistical differences between the groups, with n = 3 in each group. The area of spheroids on each day was measured using ImageJ software and is represented on the bar graph, with n = 3 (top right-end) Scale bars: 100 µm. (**B**) Representative two-dimensional migration assay images depicting the scratch at the time points mentioned above. The percentage of wound closure was measured using ImageJ software, and statistical analysis between the groups for each day was performed using two-way analysis of variance, with n = 5. (**C**) Representative image of the Boyden chamber insert used for the transwell invasion assay of HT29 WT and KO cells. The bar graph represents the quantified number of cells in each image captured and averaged. The two-tailed unpaired t-test was used to compare the groups, with n = 3 in each group. GraphPad Prism 10 was used to generate graph and perform statistical analysis with *, $p < 0.05$; **, $p < 0.005$; ***, $p < 0.0005$, ****, $p < 0.0001$ (microscope software details, magnification or zoom). MIEN1, migration and invasion enhancer 1; KO, knockout; WT, wild-type.

core, whereas HT29 WT cells struggled to create a singular spheroid with clear boundaries (Fig. 5A). These results suggest that the knockout of *MIEN1* enhances cellular adhesion among HT29 KO cells, which likely leads to a reduction in migration potential. These results imply that MIEN1 knockout amplifies cellular adhesion in HT29 KO cells, likely resulting in a diminished migration potential.

To further investigate the effect of *MIEN1* knockout on cell migration, we performed a traditional wound-healing assay. A significant 0.25-fold reduction in wound closure was observed in KO cells compared with that in WT cells (Fig. 5B).

We also examined the impact of *MIEN*1 knockout on the invasion potential of these cells. Using the Boyden chamber invasion assay, we found that HT29 KO cells displayed a remarkable 40% reduction in invasion potential compared with HT29 WT cells (Fig. 5C).

Collectively, these findings suggest that MIEN1 knockout increases cell–cell adhesion, severely limiting the migration and invasion capabilities of HT29 cells.

Discussion

MIEN1 is overexpressed in various cancers, including breast, prostate, oral, ovarian, and colorectal cancers. Our previous investigations revealed the active involvement of MIEN1 in promoting prostate cancer metastasis by activating the Akt/NF-kB pathway, thereby upregulating the transcription of matrix metalloproteases and angiogenic factors[5]. Additionally, RNA interference–mediated downregulation of *MIEN1* in prostate and breast cancer results in alterations in the actin cytoskeleton, impacting cellular movement[4,5]. However, there are limited studies on the role of MIEN1 in CRC metastasis. This study aimed to address this gap by investigating the contribution of *MIEN1* in CRC metastasis using a gene knockout model.

Previous studies have emphasized the significance of the *MIEN1* promoter region in regulating its expression. Evans et al.[7] reported that *MIEN*1 overexpression in cancer cell lines was attributed to transcriptional control rather than gene amplification. Rajendiran et al.[8] further demonstrated that hypomethylation of the SINE Alu region of the *MIEN1* promoter results in its overexpression in cancer cells. Hence, we developed a strategy to delete the minimal promoter region of *MIEN1* in the HT29 CRC cell line, ensuring the specificity of the knockout while avoiding interference with important neighboring genes such as *ERBB2* and *GRB7*. This contrasts with a method previously reported by Van Treuren et al., which involved generating a CRISPR-mediated *MIEN1* knockout in triple-negative breast cancer cells by deleting a specific segment of *MIEN1* within the *ERBB2* amplicon[9]. The absence of the *MIEN1* transcript and protein in KO cells, in contrast to its abundant expression in WT cells, validates the efficacy of our knockout strategy. While this strategy provides an effective means of investigating *MIEN1* function, complementary studies in additional CRC cell lines would strengthen the robustness of the findings.

Subsequent transcriptomic analysis revealed significant alterations in the gene expression patterns following *MIEN*1 knockout. The distinct global expression patterns between WT and KO cells emphasize the profound impact of *MIEN1* deletion on the cellular transcriptome. Various physiological functions, such as endothelial cell development, transactivation, immortalization, cytoskeletal rearrangement, and EMT, are directly or indirectly associated with malignancy advancement. Notably, reduced sperm motility was predicted to be inhibited by *MIEN1* knockout, indicating its involvement in cellular movement beyond cancer.

Rearrangement of the actin cytoskeleton is closely associated with cancer cell migration and invasion. A previous study by Dasgupta et al. identified the presence of a post-translationally modified isoprenyl group at the carboxy terminus of the MIEN1 protein, a modification also observed in other proteins involved in actin assembly, such as the Rho family[4]. Furthermore, Kpetemey et al. demonstrated that *MIEN1* overexpression leads to increased lamellipodia formation compared to cells with normal MIEN1 levels[3]. Consistent with our previous study, we report for the first time that MIEN1 knockout in CRC cells results in a significant reduction in lamellipodia formation and an increase in stress fiber accumulation in the cell bodies of HT29 cells. The substantial presence of stress fibers in *MIEN1* KO cells, as opposed to WT cells (Fig. 3A–D), indicating enhanced cell adhesion to the substratum, which inhibited cell motility. Moreover, increased phosphorylation of cofilin at serine 3 (S3) was observed, indicating its inactivation (Fig. 4E and F). This inactivation led to the inhibition of actin depolymerization, thereby promoting stress fiber formation, as demonstrated by immunofluorescence staining (Fig. 4C) These results provide key insights into the cytoskeletal functions of MIEN1; however, a more detailed exploration of its downstream signaling pathways, such as the Rho GTPase and PI3K/Akt axes, would help refine our understanding of its molecular role in CRC metastasis. Another critical actin cytoskeleton protein, FAK, is phosphorylated at tyrosine 397, and its phosphorylation is significantly affected by the absence of MIEN1. In this study, we observed a marked difference in the subcellular localization of pFAK-Y397 . In WT cells, pFAK-Y397 was prominently localized at the cellular edges, particularly along the lamellipodia. This observation is consistent with the increased phosphorylation observed in WT cells, as shown by immunoblotting. Increased phosphorylation indicates FAK activation, which in turn activates the Rac pathway, enhancing lamellipodia formation and, thereby, increasing cellular migration and invasion[1011]. This explains the recruitment of pFAK-Y397 to the cellular edges in WT cells. In contrast, pFAK-Y397 was predominantly localized within the cell body in KO cells around abundant stress fibers. Immunoblot analysis of KO cells revealed reduced FAK phosphorylation at Y397, indicating FAK inactivation. Inactive FAK maintains Rho GTPases in an inactive state, and the downregulation of the Rho GTPase pathway can inhibit cell migration and invasion, which are often associated with FAK localization in stress fibers[12]. Therefore, in the absence of lamellipodia, pFAK-Y397 is recruited to the cell body, where stress fibers are present, rather than to the cell edges. However, *MIEN1* knockout may trigger compensatory mechanisms that alter the cellular phenotype over time. Phosphoproteomics or functional rescue experiments, could help determine whether other molecules compensate for MIEN1 loss. Additionally, the alterations in actin cytoskeleton rearrangement were consistent with the results of functional assays, elucidating the impact of MIEN1 knockout on cell–cell adhesion, migration, and invasion. The enhanced cell-to-cell adhesion efficiency, coupled with the reduced wound closure and decreased invasion potential observed in KO cells, provides substantial evidence for the significant implications of *MIEN1* deletion on CRC migration and invasion potential. Importantly, a recent study by Tripathi et. al demonstrated that short peptides designed to target MIEN1 exert potent anticancer activity, supporting the promise of MIEN1 as a therapeutic target and underscoring the need for further preclinical modeling13. Importantly, a recent study by Tripathi and colleagues (2024) demonstrated thatshort peptides designed to target MIEN1 exert potent anticancer activity, supporting the promise of MIEN1 as a therapeutic target andunderscoring the need for further preclinical modeling. These findings suggest that *MIEN1* deletion may inhibit CRC metastasis. While our in vitro observations provide strong mechanistic insights, further validation in in vivo models would be crucial to assess the translational relevance of targeting MIEN1 in CRC.

In conclusion, our findings highlight the crucial role of MIEN1 in regulating the migration and invasion potential of CRC cells by influencing actin cytoskeleton dynamics. Further investigation of the compensatory signaling pathways, and validating the functional role of MIEN1 in vivo would enhance our understanding of CRC metastasis and facilitate the development of novel treatment strategies for CRC.

Materials and methods

Cell culture

HT29 cells were obtained from the ATCC (Manassas, VA, USA) (Cat. no. HTB-38). The cells were maintained at 37 °C in a 5% CO_2 incubator in HyClone McCoy's 5A medium (Cat. no. #SH30200FS) supplemented with 10% fetal bovine serum (FBS) and 1% antibiotic–antimycotic (Gibco).

CRISPR-Cas9 *MIEN1* promoter editing

HT29 WT cells were cultured and electroporated with a DNA mixture of plasmids expressing C1486_MIEN1_5′gRNA- 1, C1486_MIEN1_3′gRNA-1, and the *cas9* gene (chimeric gRNA + hSpCas9 coexpression vector, C1486_MIEN1_5′gRNA-1:5′ GCCATCAGCACCGGGCGTGG-3′, and C1486_MIEN1_3′gRNA-2:5′ CATCGCGGCCGGCTCCGCTC-3′). The region encompassing 856 bp (− 870 to − 15 bp) was deleted using the above-mentioned guide RNAs (Fig. S1). Cell selection was performed using 1.0–1.5 µg/mL puromycin for 48 h. A small portion of the cell culture (presumably containing a mixed population) was subjected to genotype analysis. The mixed culture was diluted to less than 1 cell/200 µL of culture media and dispersed into each well of a 96-well plate. The cells were allowed to grow for 15–20 days. Cells derived from single-cell cloning were subjected to genotype analysis. Positive clones for the desired mutation were cultured-expanded, and a portion was used to confirm the predicted genotype. Genotyping involves the use of genomic DNA from single-cell clones. An approximately 400-bp DNA fragment was amplified using MIEN_2F and MIEN_2R primers (MIEN_2F: 5′-GGGATGCGCAGAAACTGTTGG-3′; MIEN_2R: 5′-GTTCACTGGGGAGTCAAGAGATGG-3′). The amplicons were then subjected to direct sequencing. The obtained cell line lacking the MIEN1 promoter region was named HT29-pMIEN1-X and is referred to as HT29 KO. Applied StemCell (Applied Stem Cell Inc., Foster City, CA, USA) was used for genome editing.

RT-PCR

Total RNA was extracted using the TRIzol reagent (Invitrogen, Carlsbad, CA, USA). Superscript-III First Strand Synthesis kit (Invitrogen) was used for complementary DNA (cDNA) synthesis using 1 µg of total RNA, following the manufacturer's protocol. PCR was performed to amplify the cDNA using Taq DNA polymerase and specific primers for the target genes. The PCR cycling conditions were as follows: 95 °C for 15 min, followed by 32 cycles at 95 °C for 30 s, annealing at 54 °C for 1 min, extension at 72 °C for 45 s, and held at 4 °C. PCR products were analyzed by agarose gel electrophoresis on a 1.2% agarose gel stained with ethidium bromide. Gel images were captured using a gel documentation system.

Antibodies and reagents

The rabbit anti- p-cofilin Ser 3 (cat #3311, 1:1000), rabbit anti-cofilin (cat #5175, 1:1000), rabbit anti-HER2/ErbB2 (29D8) (cat #2165, 1:1000), were procured from Cell Signaling Technologies (Danvers, MA, USA). Purchased from Invitrogen (Waltham, MA, USA) were the rabbit anti-p-FAK (cat # 700255, 1:1000), were the rabbit anti-FAK (cat # AH00502, 1:1000). Abclonal (Woburn, MA, USA) provided rabbit anti-GRB7 (cat # A5690, 1:1000). Mouse anti-MIEN1 (cat #H00084299-M02, 1:5000) was from Abnova. Rabbit anti-HSC70 (cat # ADI-SPA-816, 1:1000) was provided by Enzo Life Sciences (Farmingdale, NY, USA). Invitrogen (Waltham, MA, USA) provided the Alexa Fluor anti Rabbit 488 antibody (cat # A11034, 1:1000), Phalloidin 594 (cat # A12381, 1:1000), and DAPI (cat # 62248, 1:1000).

Immunoblotting analysis

Proteins were extracted from cells using a radioimmunoprecipitation assay buffer (Thermo Scientific) supplemented with protease inhibitors (Millipore Sigma) and phosphatase inhibitors (Millipore Sigma), and then quantified using the BCA Protein Assay Kit (Thermo Scientific). Equal amounts of protein were loaded onto 4–12% precast SDS-PAGE gels (Invitrogen), and the samples were electrotransferred to a nitrocellulose membrane (Invitrogen) at a constant voltage of 25 V. The blots were then blocked with 5% bovine serum albumin (Thermo Scientific) and incubated with the respective primary antibodies at 4 °C for 8–10 h, followed by incubation with the respective secondary antibodies tagged with horseradish peroxidase. Protein bands were visualized using the Alpha Innotech Chemiluminescent Detection System and the iBright CL1500 Imaging System (Thermo Scientific).

RNA sequencing

Library construction and sequencing

RNA sequencing libraries were prepared using the Illumina Stranded mRNA Library Prep kits (Cat. no. 20040534), following the manufacturer's instructions. Briefly, 1 µg of total RNA was used as the starting material. Poly(A)-tailed RNA was purified using poly(T) oligo beads included in the kit. The resulting RNA samples were then fragmented and converted into double-stranded DNA for sequencing. Individual libraries were uniquely indexed using Illumina RNA UD Indexes (Cat. no. 20040555) and pooled at an equimolar ratio. The pooled libraries were sequenced on an Illumina NextSeq 550 sequencing system to obtain 75-bp paired-end reads. Raw sequence reads were deposited in the Sequence Read Archive with the reference ID PRJNA1218296 in GenBank. RNA sequencing was performed using the Genomics Core at the UNT Health Science Center.

Read mapping and gene expression analysis

The quality of the raw FASTQ files was evaluated using the Galaxy web-based platform. Subsequently, adaptor trimming was performed using Trim Galore software. The trimmed files were merged into one file for R1 and R2 using text manipulation by concatenating the datasets from tail to head. The merged FASTQ files were then aligned to the human genome build GRCh38-Ensembl using HiSat2. Mapped BAM files were run using feature counts to obtain gene counts, which were then run using DEseq2 to identify differentially expressed genes.

Gene ontology and gene set enrichment analysis

Gene ontology analysis was performed using QIAGEN's IPA software with features such as network analysis, upstream regulator analysis, pathway analysis, and canonical pathway analysis, with a P-value cut-off set to 0.05.

Wound-healing assay

3×10^5 cells were seeded in 6-well culture plates and incubated at 37 °C and 5% CO_2 until they reached 80% confluency. The cells were then serum-starved for 24 h prior to creating a wound for cell cycle synchronization. A straight wound was created using a 100-µL pipette tip. Floating cells were removed by washing with 1 × phosphate-buffered saline (PBS). The cells were incubated in McCoy's 5A medium (HyClone) with 10% FBS and 1% antibiotic–antimycotic at 37 °C in 5% CO_2. Wound-healing images were acquired over 24 h at equal intervals using a Keyence AIO BXZ-X810 inverted fluorescence microscope. ImageJ software (v.2.14.0) (https://imagej.net/ij/) was used to quantify the gaps in the cell monolayers.

Transwell invasion assay

Boyden chambers with a transwell membrane of 8-µm pore size (Corning, NY, USA) were seeded with 3×10^5 cells/well in 200-µL serum-free McCoy's 5A medium. Next, 500 µL of McCoy's 5A medium (HyClone) with 10% FBS and 1% antibiotic–antimycotic were added to the wells of a 24-well plate and incubated for 48 h at 37 °C in 5% CO_2. The Boyden chambers were stained with 0.05% crystal violet after fixation with 4% paraformaldehyde. Uninvaded cells were removed using cotton swabs, and the number of invaded cells was counted using phase-contrast microscope – Nikon Eclipse Ti–U.

Hanging-drop assay

A total of 2×10^5 cells/mL were seeded on the lid of a 90-mm dish in six 20 µL drops. Next, 7 mL of 1× PBS was added to a 90-mm dish, and the lid was carefully inverted on the dish. Images were captured every 24 h for 4 days.

Immunofluorescence staining

The cells were seeded on 22-mm coverslips, fixed in 4% paraformaldehyde (Thermo Scientific) for 15 min at room temperature, and permeabilized with 0.1% Triton X-100 (Sigma) for 15 min at room temperature. Blocking was performed using 5% goat serum (Invitrogen) for 1 h at room temperature, followed by overnight incubation at 4 °C with the respective primary antibodies. After primary incubation, the cells were rinsed three times with 1 × PBS containing Tween 20 and subsequently incubated with the respective secondary antibodies for 1 h at room temperature. Next, the cells were incubated with 4',6-diamidino-2-phenylindole for 10 min at room temperature, followed by mounting on slides using a mounting medium (Invitrogen). Images were acquired using an Inverted Zeiss LSM 880 Airyscan confocal microscope.

Statistical analysis

The statistical analysis of all the data was done with GraphPad Prism 10 (La Jolla, CA, USA). Every experimental result was obtained from a minimum of three separate experiments. One-way ANOVA or t-tests, as required for the experiment, were used to evaluate statistical significance. A statistically significant result was defined with reference to $P <$ as mentioned in the figure legends.

Data availability

The datasets generated and/or analyzed during the current study are available in the Sequence Read Archive (SRA) data repository, under accession number PRJNA1218296. Further inquiries can be forwarded to the corresponding author.

Received: 4 April 2025; Accepted: 13 August 2025
Published online: 29 September 2025

References

1. Amin, M. B. et al. The eighth edition ajcc cancer staging manual: Continuing to build a bridge from a population-based to a more "personalized" approach to cancer staging. *CA Cancer J. Clin.* **67**, 93–99 (2017).
2. Cappell, M. S. Pathophysiology, clinical presentation, and management of colon cancer. *Gastroenterol. Clin. North Am.* **37**, 1–24 (2008).
3. Kpetemey, M., Chaudhary, P., Van Treuren, T. & Vishwanatha, J. K. MIEN1 drives breast tumor cell migration by regulating cytoskeletal-focal adhesion dynamics. *Oncotarget* **7**, 54913–54924 (2016).
4. Dasgupta, S., Cushman, I., Kpetemey, M., Casey, P. J. & Vishwanatha, J. K. Prenylated C17orf37 induces filopodia formation to promote cell migration and metastasis. *J. Biol Chem.* **286**, 25935–25946 (2011).
5. Dasgupta, S. et al. Novel gene C17orf37 in 17q12 amplicon promotes migration and invasion of prostate cancer cells. *Oncogene* **28**, 2860–2872 (2009).
6. Dong, X. et al. C35 is overexpressed in colorectal cancer and is associated tumor invasion and metastasis. *Biosci Trends.* **9**, 117–121 (2015).
7. Evans, E. E. et al. C35 (C17orf37) is a novel tumor biomarker abundantly expressed in breast cancer. *Mol. Cancer Ther.* **5**, 2919–2930 (2006).
8. Rajendiran, S., Gibbs, L. D., Van Treuren, T., Klinkebiel, D. L. & Vishwanatha, J. K. MIEN1 is tightly regulated by SINE Alu methylation in its promoter. *Oncotarget* **7**, 65307–65319 (2016).
9. Van Treuren, T. & Vishwanatha, J. K. CRISPR deletion of MIEN1 in breast cancer cells. *PLoS ONE* **13**, e0204976 (2018).
10. Sylow, L. Tyrosine 397 phosphorylation is critical for FAK-promoted Rac1 activation and invasive properties in oral squamous cell carcinoma cells. *Lab Invest.* **96**, 1026 (2016).
11. Schober, M. et al. Focal adhesion kinase modulates tension signaling to control actin and focal adhesion dynamics. *J Cell Biol.* **176**, 667–680 (2007).
12. Magalhaes, Y. T., Boell, V. K., Cardella, G. D. & Forti, F. L. Downregulation of the Rho GTPase pathway abrogates resistance to ionizing radiation in wild-type p53 glioblastoma by suppressing DNA repair mechanisms. *Cell Death Dis.* **14**, 283 (2023).

13. Amit K., Tripathi Priyanka P., Desai Antariksh, Tyagi Jana B., Lampe Yogesh, Srivastava Michael, Donkor Harlan P., Jones Sergei V., Dzyuba Eric, Crossley Noelle S., Williams Jamboor K., Vishwanatha. Short peptides based on the conserved regions of MIEN1 protein exhibit anticancer activity by targeting the MIEN1 signaling pathway. *Journal of Biological Chemistry* **300**(3), 105680 https://doi.org/10.1016/j.jbc.2024.105680 (2024).

Acknowledgements
We acknowledge the UNTHSC Genomics and Microscopy Core for their support with RNA sequencing and immunofluorescence imaging. We extend our appreciation to Dr. T. Kwon at the UNTHSC Genomics Core for his assistance with RNA sequencing, and to Mr. Kishor Kunwar at the HSC Microscopy Core for his training and support with immunofluorescence imaging. We sincerely thank Dr. Amit Kumar Tripathi for his scientific advice.

Author contributions
P.R. designed the study, performed the experiments and data analysis, and wrote the manuscript. D.C.S.D and P.L. generated the knockout cell line. R.T. assisted in experiments and contributed to the manuscript writing. J.K.V. conceptualized and supervised the study and acquired funding. All authors have edited and revised the manuscript and approved the final version.

Funding
This work was supported by awards from the National Institute of Health under awards R01CA220273, U54MD006882 and S21MD012472 and from the Cancer Prevention and Tesesrch Institute of Texas award number RP210046 to Dr. Jamboor K. Vishwanatha. The MIEN1 knockout cells were generated through an award from Universidad del Rosario (Grant: CS/ABN062/GENIUROS 018–019).

Declarations

Competing interests
The authors declare no competing interests.

Additional information
Supplementary Information The online version contains supplementary material available at https://doi.org/10.1038/s41598-025-16124-z.

Correspondence and requests for materials should be addressed to J.K.V.

Reprints and permissions information is available at www.nature.com/reprints.

Publisher's note Springer Nature remains neutral with regard to jurisdictional claims in published maps and institutional affiliations.

Open Access This article is licensed under a Creative Commons Attribution-NonCommercial-NoDerivatives 4.0 International License, which permits any non-commercial use, sharing, distribution and reproduction in any medium or format, as long as you give appropriate credit to the original author(s) and the source, provide a link to the Creative Commons licence, and indicate if you modified the licensed material. You do not have permission under this licence to share adapted material derived from this article or parts of it. The images or other third party material in this article are included in the article's Creative Commons licence, unless indicated otherwise in a credit line to the material. If material is not included in the article's Creative Commons licence and your intended use is not permitted by statutory regulation or exceeds the permitted use, you will need to obtain permission directly from the copyright holder. To view a copy of this licence, visit http://creativecommons.org/licenses/by-nc-nd/4.0/.

© The Author(s) 2025